

LA UR 82-3346

Conf-320725--4

Los Alamos National Laboratory is operated by the University of California for the United States Department of Energy under contract W-7405-ENG-36.

LA-UR--82-3346

DE83 003643

TITLE:

MATERIALS RESPONSE TO LARGE PLASTIC DEFORMATION

AUTHOR(S):

M. G. Stout and S. S. Hecker


SUBMITTED TO:

29th Sagamore Army Materials Research Conference -- Proceedings  
Lake Placid, NY, held July 19-23, 1982

NOTICE

**PORTIONS OF THIS REPORT ARE ILLEGIBLE. It  
has been reproduced from the best available  
copy to permit the broadest possible avail-  
ability.**

DISCONTINUED PUBLICATION

By acceptance of this article, the publisher  agrees that the U.S. Government retains a nonexclusive, royalty free license to publish or reproduce the published form of this contribution, or to allow others to do so, for U.S. Government purposes.

The Los Alamos National Laboratory requests that the publisher identify this article as work performed under the auspices of the U.S. Department of Energy.

**Los Alamos** Los Alamos National Laboratory  
Los Alamos, New Mexico 87545

## MATERIALS RESPONSE TO LARGE PLASTIC DEFORMATION

M. G. Stout and S. S. Hecker

Materials Science and Technology Division  
Los Alamos National Laboratory  
Los Alamos, N.M. 87545

### INTRODUCTION

Many important practical applications of metals require a knowledge of the plastic response at large deformations and at high strain rates. For example, metal forming processes and impact or penetration problems combine the effects of large strain, high rate and temperature. Accurate modeling of such processes requires a good constitutive description of material behavior. However, controlled laboratory experiments at large strains are difficult because most involve large geometry changes accompanied by either deformation gradients (such as barreling in compression) or plastic instability (such as necking in tension). High rate deformation adds the complication of an uncontrolled temperature rise. In the strain rate regime of 1 to  $10^7$  sec<sup>-1</sup>, deformation may be neither completely isothermal nor adiabatic, but a combination.

Because of these experimental complications few good laboratory experiments have been conducted at high rates to large plastic strains. Lindholm describes some high rate torsion results in this volume. In this paper, we concentrate on large strain behavior without the complication of high rates. Gil Sevillano, van Houtte and Aernoudt have recently published a comprehensive review of large strain deformation. We are adding some of our recent experimental results to a review we presented at a recent workshop.

#### DISCLAIMER

This document contains information that is classified "Secret" under Executive Order 12958, Section 1.5, and is exempt from automatic downgrading and declassification. This document is the property of Los Alamos National Laboratory and is loaned to your organization. It and its contents are not to be distributed outside your organization. If you are no longer an employee of Los Alamos National Laboratory, you are not to disseminate, distribute, or use this information in any way. If you have any questions concerning this document, please contact the Los Alamos National Laboratory Information Office, P.O. Box 16633, Los Alamos, NM 87545.

12/18  
DISTRIBUTION OF THIS DOCUMENT IS UNLIMITED

## REVIEW OF EXPERIMENTAL TECHNIQUES

Uniaxial tension is restricted to small strains by plastic instability (necking). Few metals can stretch more than 50% before necking. Early attempts to remachine specimens to remove the neck have not become popular. With the advent of closed loop testing machines it has become more popular to use a diametral extensometer at the neck to control the tensile test with diametral strain. Area and triaxial stress correction are then used to reconstruct a uniaxial tensile curve.<sup>3,4</sup> This method involves a number of assumptions and has yet to be proven. Uniaxial compression is limited by barreling and end effects from the platen. To achieve a true uniaxial stress state excellent lubrication and a length/diameter ratio of  $\sim 1.6$  are required. Large changes in geometry require remachining, which has been practiced much more extensively in compression than in tension. It obviously requires starting with a very large specimen. We will present some data of interrupted compression tests to strain levels of 4.

Biaxial tension experiments on sheet material are able to produce effective strain levels approximately twice those attainable in uniaxial tension. The added stability<sup>5-8</sup> under biaxial tension has been discussed by a number of authors. Hydraulic bulging offers the best experimental technique for stress-strain measurements of sheet specimens. Unfortunately, there is considerable controversy over the potential errors introduced by small bulge diameters,<sup>9,10</sup> biaxial extensometers, and varying strain rates during bulging. A much more accurate and versatile technique for biaxial tension is the axial loading/internal pressurization of thin-walled tubes. However, geometric instabilities limit the strain levels<sup>11</sup> to values even lower than those attainable in uniaxial tension.

Torsional deformation offers the best hope for large-strain experiments because it is accompanied by very small geometry changes. However, torsion also suffers from several important restrictions. Experimentally, specimens elongate during torsion and care must be exercised not to restrain their length. Torsion of solid rods also produces an inherently non-uniform stress state, varying from zero at the axis to a maximum at the surface. There has been considerable discussion over the years about how to properly convert a measured torque/angle curve to an effective stress/effective strain curve.<sup>12,13</sup> Much of the torsional data in the literature is inconsistent because of the

different methods of analysis employed. Most recently, Canova et al.<sup>14</sup> have developed a technique using several specimens of slightly different diameters to establish an accurate stress-strain curve. The torque-angle conversion to stress-strain is simpler for thin-walled tubes, but torsional buckling limits the strain levels attainable. Apparently some large strain tests have been conducted successfully on very short tubes<sup>15</sup> without adverse end effects.

Most of the large-strain information available in the literature was obtained by indirect tests. These tests are conducted by imparting large prestrains in a deformation mode relatively insensitive to plastic instability (such as wire drawing or sheet rolling) and then testing the prestrained samples in tension. Tensile tests define a stress-strain curve as shown for our rolling + tension experiments on 1100 aluminum in Fig. 1. Because sheet rolling approximates a state of plane strain it is necessary to adjust the rolling prestrain to an effective strain. We used the von Mises effective strain criterion which gives the correction of  $\epsilon_{eff} = 1.155 \times \epsilon_c$ , where  $\epsilon_c$  is the thickness strain during rolling. Similar curves can be constructed for wire and strip drawing. For the case of wire drawing the reduction in area equals the effective strain. Although very large strains have been achieved by these techniques (up to 7 in rolling + tension and 10 in wire drawing + tension), these techniques have some obvious drawbacks. The tests are not direct; deformation is incurred under one stress state and the flow stress measured under another. Tests are also interrupted and, in many cases, require remachining of specimens. An effective strain criterion must be assumed for proper comparison and, in some cases, the deformation zone geometry may change during the very large prestrains. The large deformation also affects the development of crystallographic texture. Nevertheless, these tests have been used extensively to provide a measure of hardening at large strains.

We will focus on low strain rate data obtained by methods discussed above. From these data we hope to show trends which are also important for large strain, high strain rate predictions. Specifically, we will address the influence of deformation mode, crystal structure, material purity, and alloying on stress-strain behavior.

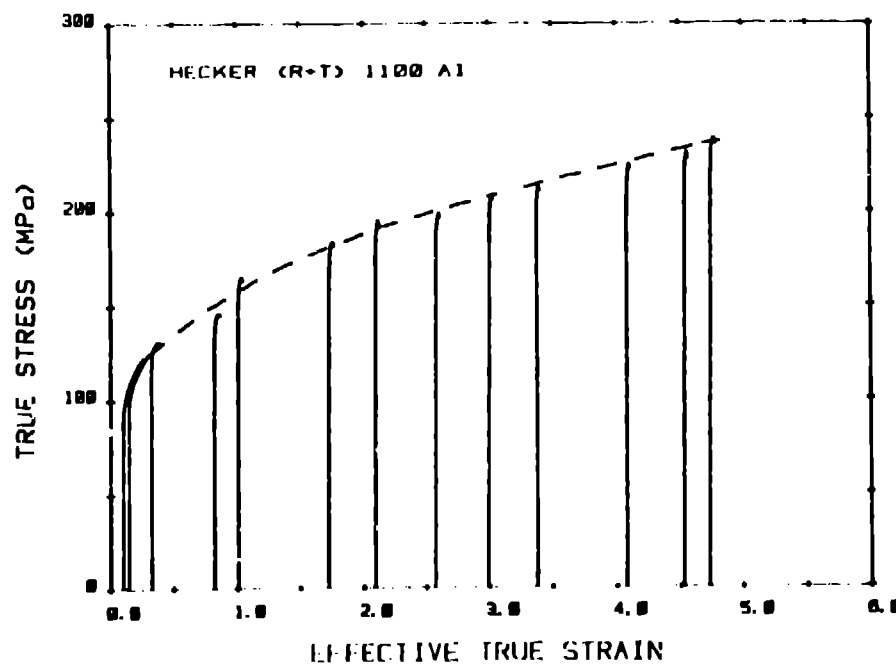


Fig. 1. Construction of a flow stress curve from rolling pre-strain followed by uniaxial tension (R+T). The thickness reduction is converted to a von Mises effective strain.

## RESULTS

### Aluminum and Aluminum Alloys

Our large strain deformation results for commercially pure aluminum are shown in Fig. 2. Tests were performed by tension, rolling + tension (R+T), and incremental compression. Hardening continues to very large strains with no evidence of saturation. The flow curve for R+T is described accurately by the parabolic hardening expression  $\sigma = 155 \epsilon^{0.2}$  (MPa). The hardening rate in compression appears somewhat lower at large strains, but these data showed considerable scatter. Hence, there appears to be very little dependence on deformation mode.

However, no torsion data for this lot of material are available for comparison.

LeFevre and coworkers<sup>18,19</sup> measured the flow behavior of a variety of aluminums of different purities using the technique of wire drawing + tension (WD+T). Some of these results are illustrated in Fig. 3 along with results of Luthy et al.<sup>20</sup> for very high purity aluminium tested in torsion at  $-20^{\circ}\text{C}$ . The results clearly show the strong influence of purity on hardening rates and flow stress levels. High purity leads to saturation, regardless of deformation mode. We believe that the major role of impurities at large strains is to impede the dynamic recovery process. Without impurities dislocation annihilation occurs readily and balances dislocation multiplication to produce a steady state saturation flow stress.

Alloying can produce a variety of behavior. The results of Lloyd and Kenny<sup>23</sup> on Al-6% Ni exhibit saturation at relatively small strains (Fig. 4). The addition of nickel results in a

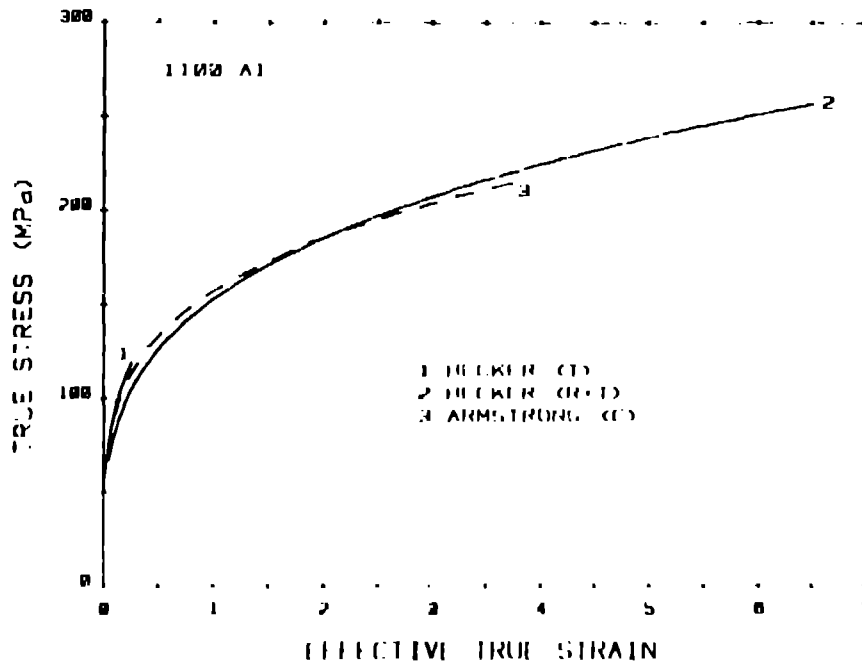


Fig. 2. Comparison of stress-strain curves as determined by tension, rolling + tension, and compression of 1100 aluminum. (References 16 and 17.)

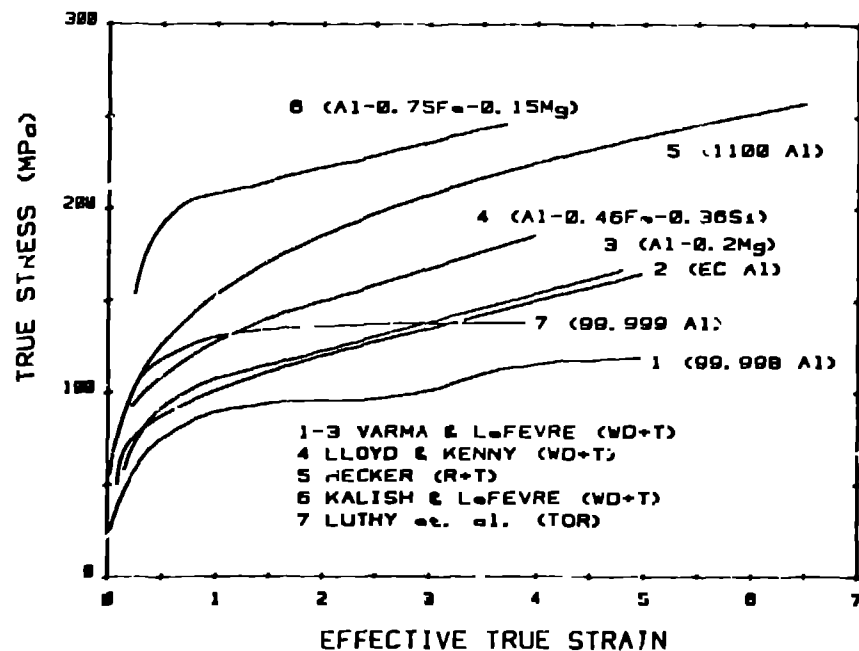


Fig. 3. Stress-strain curves for aluminum of different purities. (R+T) denotes rolling + tension and (WD+T), wire drawing + tension. (References 16-20.)

very fine dispersion of  $Al_3Ni$  which restricts the grain size during annealing. This fine dispersion of precipitates causes very rapid initial hardening followed by saturation and work softening. The role of these precipitates at large strains is not clear. They appear to restrict substructural refinement and result in very clean subgrain boundary formation. Figure 4 illustrates that both torsion and wire drawing deformation modes cause saturation. The flow stress in torsion is consistently less than that in WD+T.

The results of Nourbakhsh and Nutting<sup>22</sup> on Al-4% Cu (Fig. 4) demonstrate the importance of heat treatment and microstructure. Alloys of Al-4% Cu were heat treated to three different microstructures: to produce 1) a supersaturated solid solution of Cu in Al (Curve 1), 2) GP zones (Curve 2), and 3)  $\theta'$  precipitates (Curve 3). The hardening of the supersaturated solid solution continues at all strain levels, similar to Al-5% Mg. The alloy with GP zones showed initial hardening to a much

higher flow stress because of the GP zones contribution. However, at larger strains the GP zones were disrupted and the extra hardening increment lost. Hence, the flow stress actually leveled off and approached that of the supersaturated alloy at strains of 0.3. However, at this stress level the dislocations cut through the  $\theta'$  precipitates and the flow stress decreases. Work softening stops at a strain of  $\sim 1$ , where most  $\theta'$  precipitates are cut to result in a fine dispersion, at which point hardening resumes at a rate similar to the supersaturated alloy.

Lloyd<sup>24</sup> has also determined the effect of different initial grain sizes on the same Al-6% Ni alloy, Fig. 5. The influence of the initial grain size remains even to large strains. This indicates that initial grain size contributes to plastic behavior not only at small strains (Hall-Petch) but that it must also influence dislocation substructure development.

### Copper

The large-strain flow behavior of copper for a variety of purities and a number of deformation modes is shown in Fig. 6. Again a tendency towards saturation for high-purity copper is evident. Only the low-purity ETP copper and phosphorus-deoxidized copper exhibit distinct, continued hardening. The two curves plotted for the data of Cairns et al.<sup>27</sup> represent their and our interpretation of their data. The highest purity (99.999% Cu) copper of Truckner and Mikkola<sup>28</sup> saturates at a very low stress level at a low strain.

The effect of deformation mode on the stress-strain behavior of copper is shown in Fig. 7. Although these data are from different material heats they indicate a lower flow stress for torsional deformation. For both axisymmetric and plane strain deformation there is a tendency towards saturation.

### Nickel

Two large-strain flow curves for 200 nickel<sup>21,30</sup> are plotted in Fig. 8. Both curves are for R+T experiments. They show a plateau in flow stress between strains of 3.0 and 4.5. After a strain of 4.5 hardening continues with no tendency towards saturation. There is an absence of high purity nickel data, thus we do not know if nickel displays the same impurity effects as those found in aluminum and copper, where commercially pure



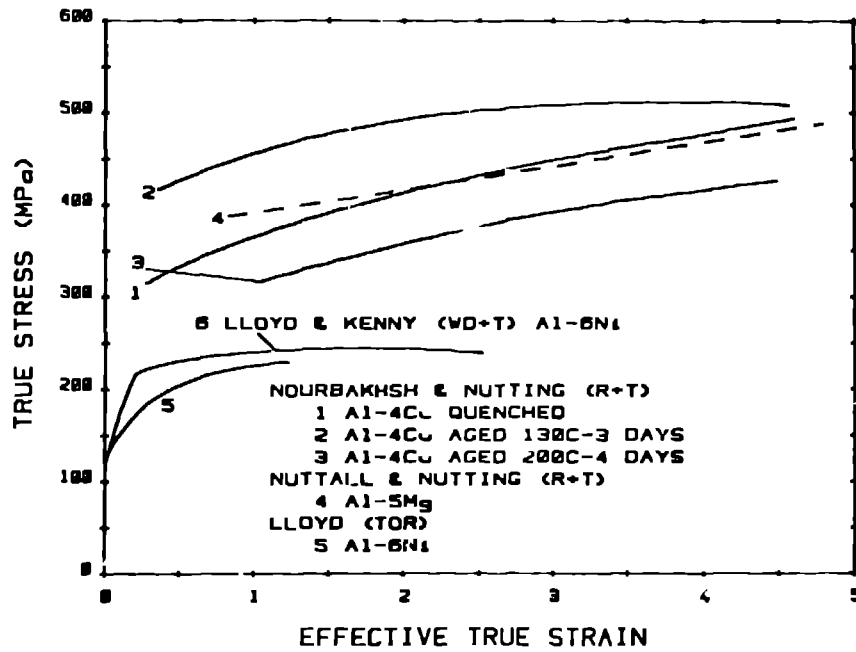


Fig. 4. Stress-strain curves for various aluminum alloys. (References 21-24.)

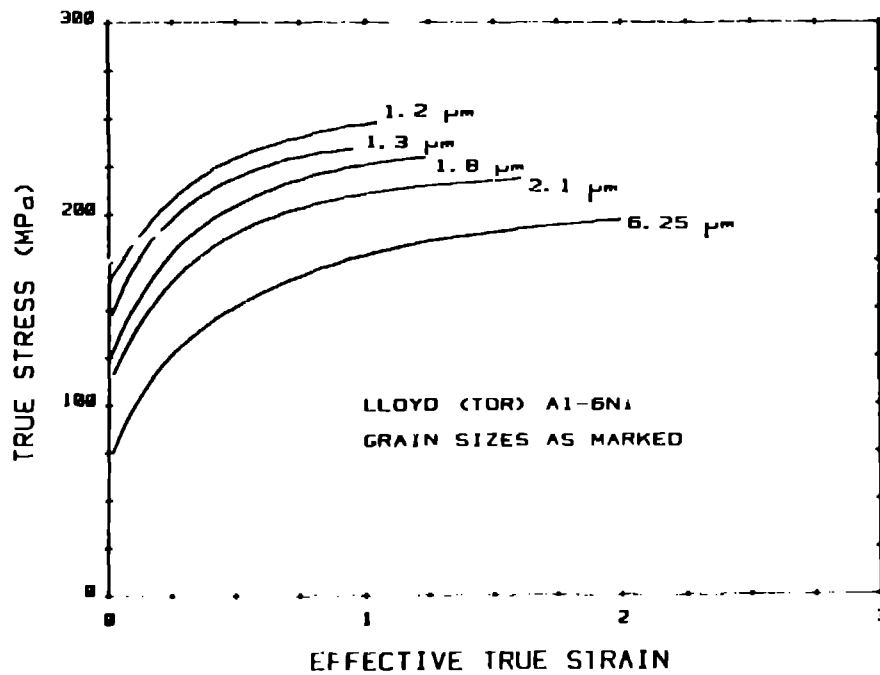


Fig. 5. Stress-strain curves of Al-6% Ni at different grain sizes as marked. (Reference 24.)

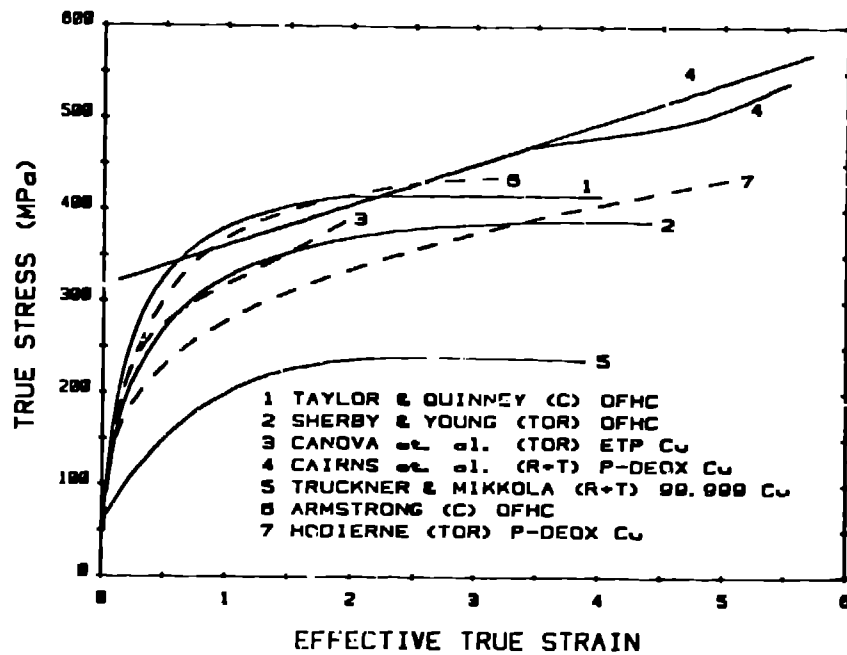


Fig. 6. Stress-strain curves for copper of different purities. (References 14, 15, 25-29.)

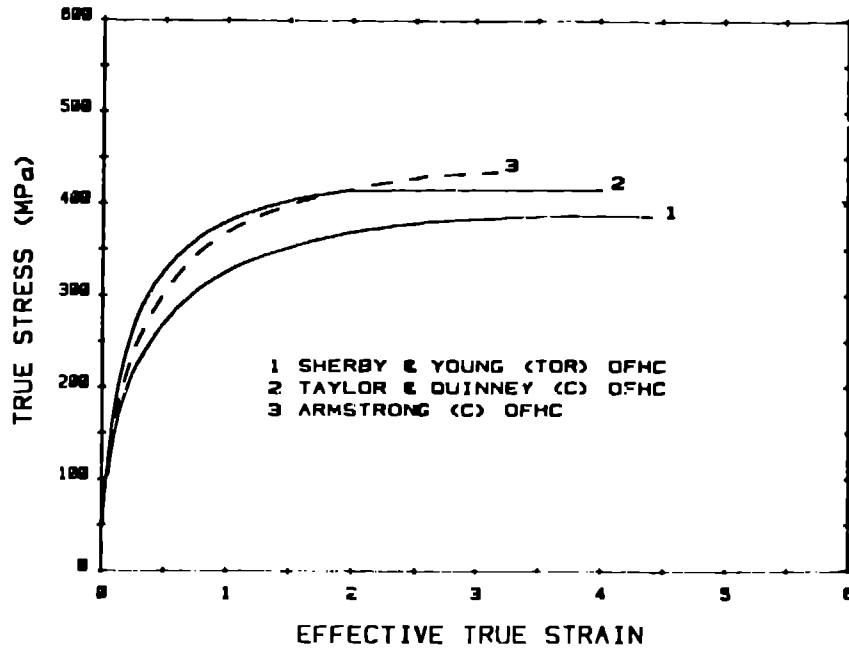


Fig. 7. Stress-strain curves for copper comparing compression versus torsion stress-strain curves. (References 25, 26, 29.)

material continues to harden while the high purity material shows a saturation.

We postulate that the return of hardening at  $\epsilon = 4.5$  might result from a initial grain size effect as pictured schematically in Fig. 9. At moderate strain levels the formation of cells and subgrains limits the dislocation mean free path. It is well established experimentally that these substructural dimensions decrease much less rapidly than the imposed grain size change. Hence, it is conceivable that grains become the limiting element again at very large strains (particularly in rolling where the imposed shape change on the through-thickness grain dimension is very rapid). The behavior of nickel in Fig. 8 may represent such a case. To date though no one has presented convincing microscopic evidence for such a transition.

#### 70-30 Brass

Experimentally the forming limit diagram of 70-30 brass has less biaxial and plane strain ductility than is predicted by a Marciniak analysis.<sup>5</sup> Ghosh<sup>31</sup> explained this in terms of a lower work hardening exponent for plane strain deformation. The plane strain work hardening exponent was determined from plane strain punch stretching and plane strain tensile data shown in Fig. 10. Most recently Wagoner<sup>32</sup> has found similar effects. We have conducted internal pressure-tension and torsion experiments with 70-30 brass tubes to investigate the stress-strain behavior in a variety of stress states. The results are plotted in terms of von Mises stress and strain in Fig. 11.

The strain levels for tension-internal pressure tests were limited by early plastic instability.<sup>11</sup> The flow stress levels for uniaxial and biaxial tension are similar, although the hardening rate in biaxial tension is slightly lower. Flow stress levels are lowest for hoop tension. Plane strain tension (both hoop and axial plane strain) is identical to torsion; the flow stress levels are intermediate between uniaxial and hoop tension, and the hardening rate is the lowest. We have made preliminary attempts to relate the flow curves to texture and microstructure. To date we have not found substantial substructural differences. For example, at an effective strain level of 0.4 both uniaxial and plane strain tension deformation exhibit ~15 percent volume fraction of twins. However, pole figure measurements indicate that the flow curves are qualitatively consistent with the initial textures.

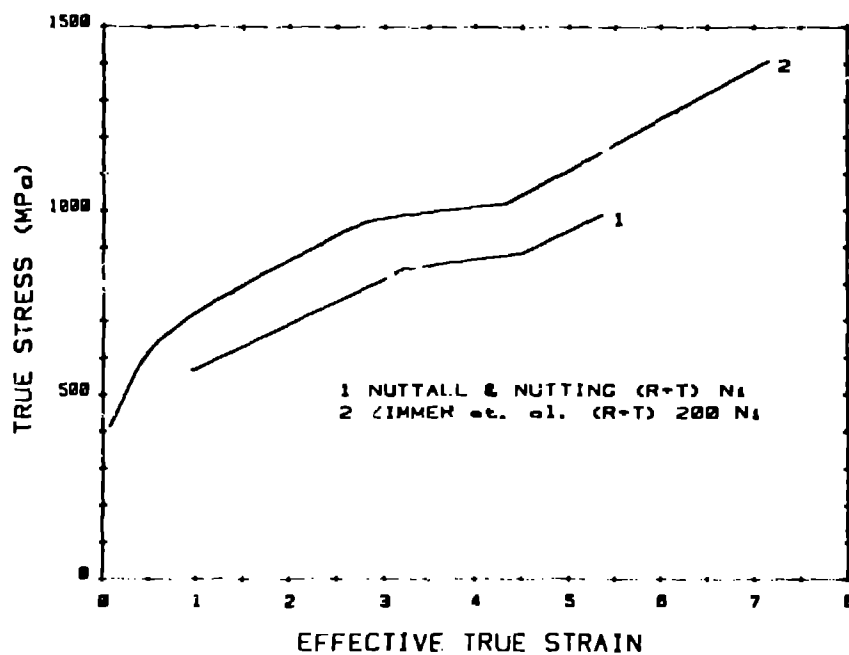


Fig. 8. Stress-strain curves for nickel. (References 21, 30.)

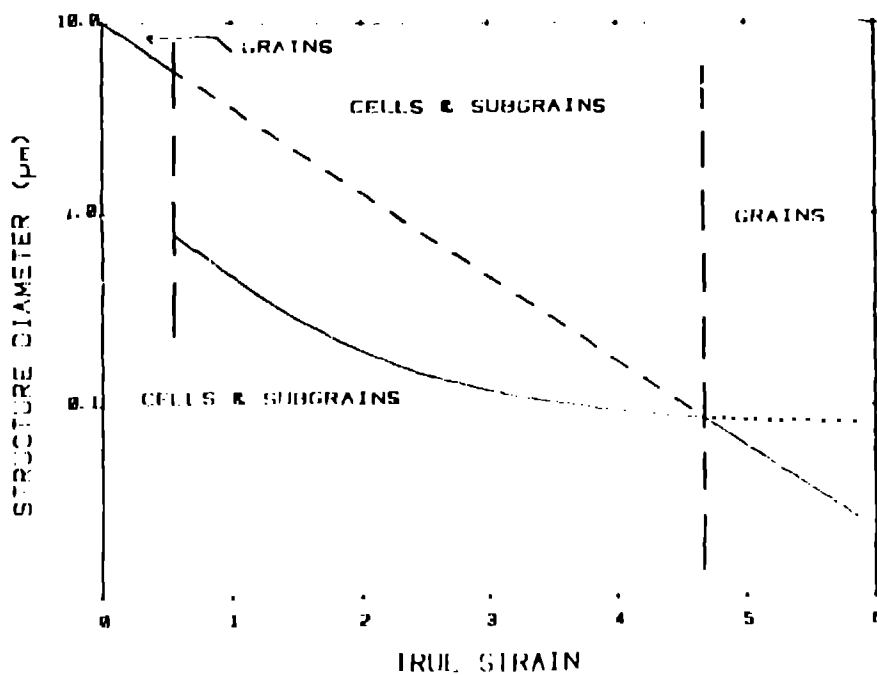


Fig. 9. The potential role of grain and substructure sizes controlling the flow stress. (Reference 1.) The dashed diagonal line represents the imposed decrease in transverse grain size by the external shape change due to rolling. The solid curve for cells and subgrains is schematic, but typical for most materials.

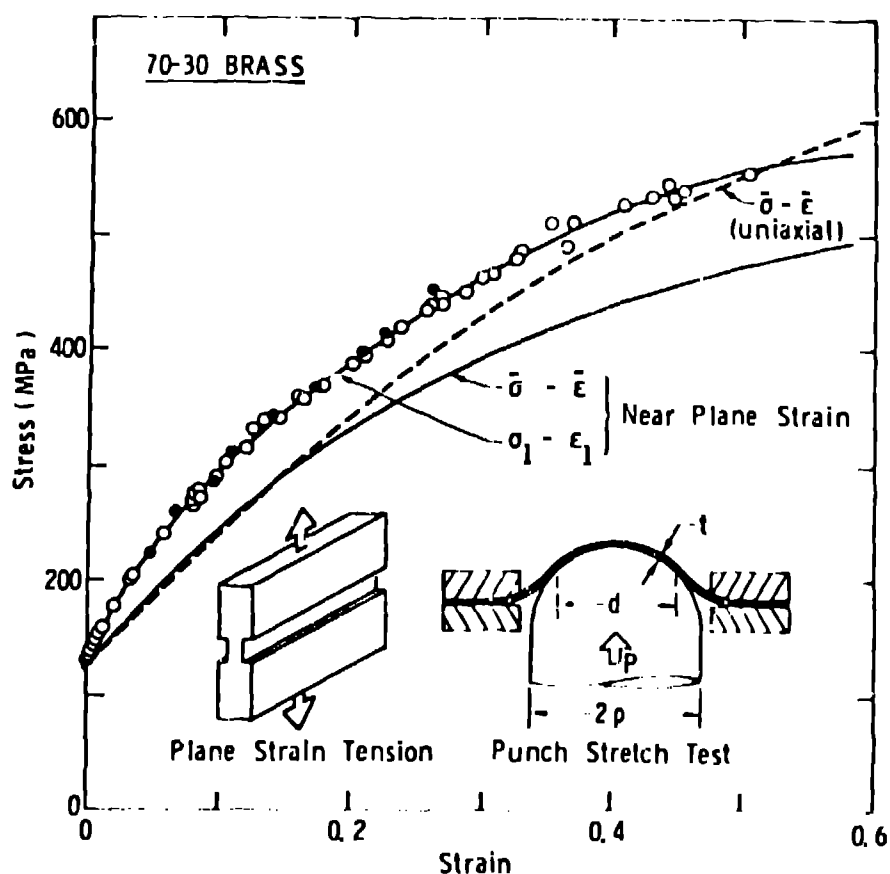


Fig. 10. Axial stress-strain data points from two biaxial tests on brass: (i) plane strain tension ( $\epsilon_2/\epsilon_1 \sim 0$ ), indicated by open circles, and (ii) punch stretch test ( $\epsilon_2/\epsilon_1 \sim 0.1$ ), indicated by solid circles. The effective stress-strain curves drawn from these data exhibit substantial difference in the rate of hardening from that of uniaxial tension. (Reference 31.)

We extended the flow curves to large strains in two different deformation modes; torsion of short gage section thin-walled tubes and uniaxial compression performed incrementally with periodic remachining. The results are shown in Fig. 12 and compared to uniaxial tension. The difference between axisymmetric, uniaxial tension (compression) and plane strain (torsion) continues to large strains. We are currently looking for a microstructural or textural explanation for this difference.

#### BCC Iron and Iron Alloys

Most of the available literature on bcc metals and alloys was summarized by GVA. We will present only the highlights here. Perhaps the most dramatic of the bcc results are shown in

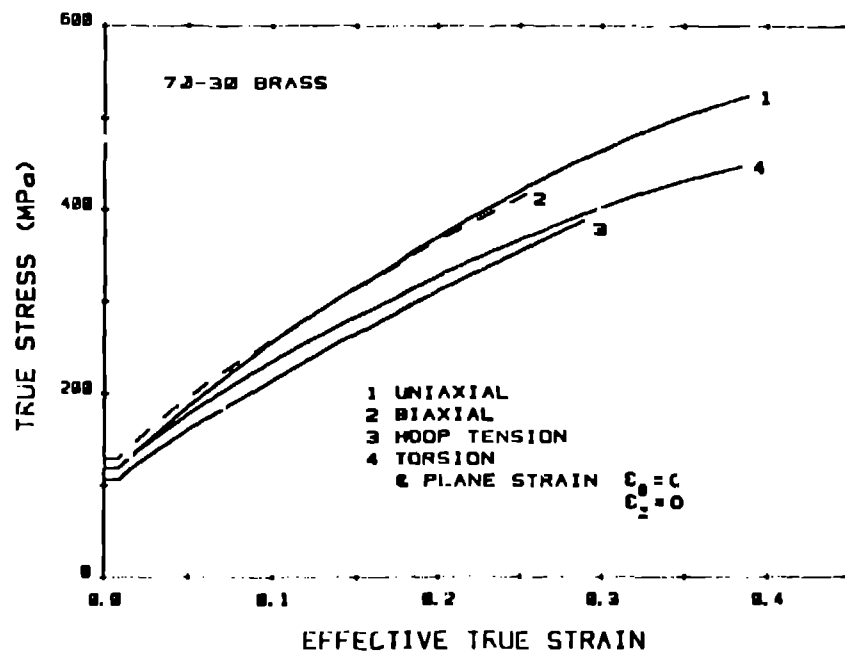


Fig. 11. Stress-strain curves for 70-30 Brass obtained from tension-internal pressure, and torsion loadings of thin-walled tubes. Note:  $\epsilon_z = 0$  is a plane strain state with no length change.  $\epsilon_\theta = 0$  is a plane strain state with no change in the hoop dimension.

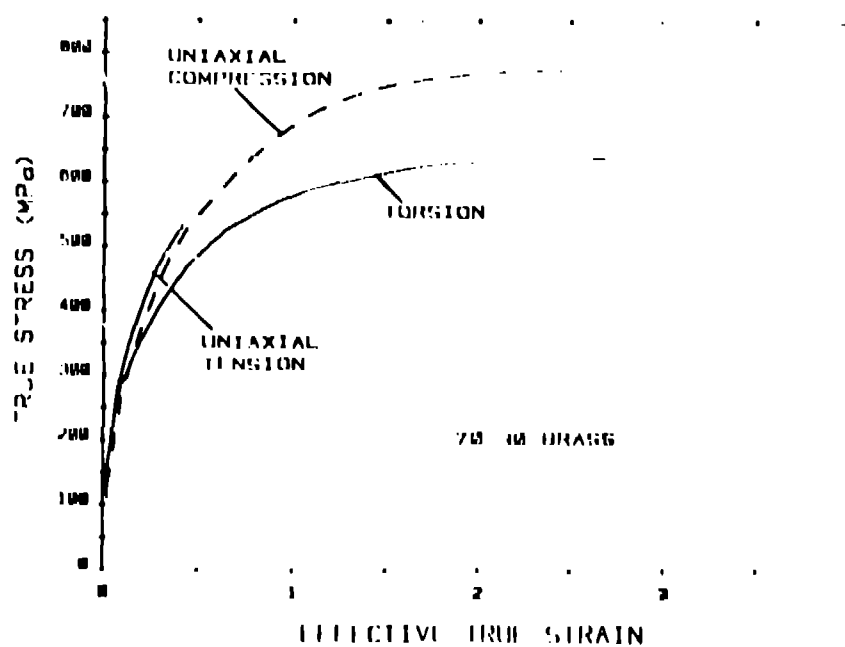


Fig. 12. A comparison of torsion (on thin-walled) tubes and uniaxial compression (on solid bars) stress-strain data for 70-30 Brass to an effective strain of 2.5.

Fig. 13. Young et al.<sup>33</sup> demonstrated the remarkable difference in hardening behavior of titanium-gettered iron (Fe-0.17% Ti) tested in torsion compared to WD+T. Hardening in torsion (solid rod data converted on the basis of the von Mises criterion) saturates, whereas hardening in WD+T is linear ( $\sigma = K\epsilon$ ) at large strains. More recent studies by Razavi and Langford<sup>34</sup> confirm the importance of deformation mode. As shown in Fig. 14, the hardening curve for strip drawing followed by tension (SD+T) appears at higher flow stress levels than WD+T, but starts to saturate at a strain similar to the torsion results. These results are similar to those reported for eutectoid steels by Aernoudt and Gil Sevillano.<sup>35,36</sup>

The explanation for this mode sensitive behavior is still being contested. Several investigators have attributed the difference to texture development. Gil Sevillano and Aernoudt claim that most deformation modes lead to hardening and that torsion represents the unusual case. They maintain that because of the texture developed in torsion the slip distance remains unchanged at moderate strains and at large strains dynamic recovery<sup>34</sup> actually increases the slip distance. Razavi and Langford<sup>34</sup> relate the continued hardening during wire drawing to redundant strain (curling of grains) necessary to maintain grain continuity. In strip drawing and torsion, deformation may be accommodated by cooperative rearrangements such as shear banding, leading to a lower hardening rate. They suggest that the decline in hardening in strip-drawn iron is a result of achieving textural and microstructural stability. Young, Anderson, and Sherby<sup>33,37</sup> explain the difference in hardening between wire drawing and torsion on the basis of substructure. In wire drawing the cells and subgrains continued to be refined and the perfection of the walls increased, whereas in torsion their size saturates. They were able to correlate the flow stress in both cases with the subgrain size and, hence, suggest that texture plays only a secondary role. However, substructural development may well depend on textural evolution and, hence, texture development may still hold the key to the dramatic differences in response between fcc and bcc metals and alloys to different modes of deformation.

Weertman and Hecker<sup>40</sup> suggested that the flow stress at large strains is governed by the character of dislocations. In torsion most of the slip occurs on systems with a common slip

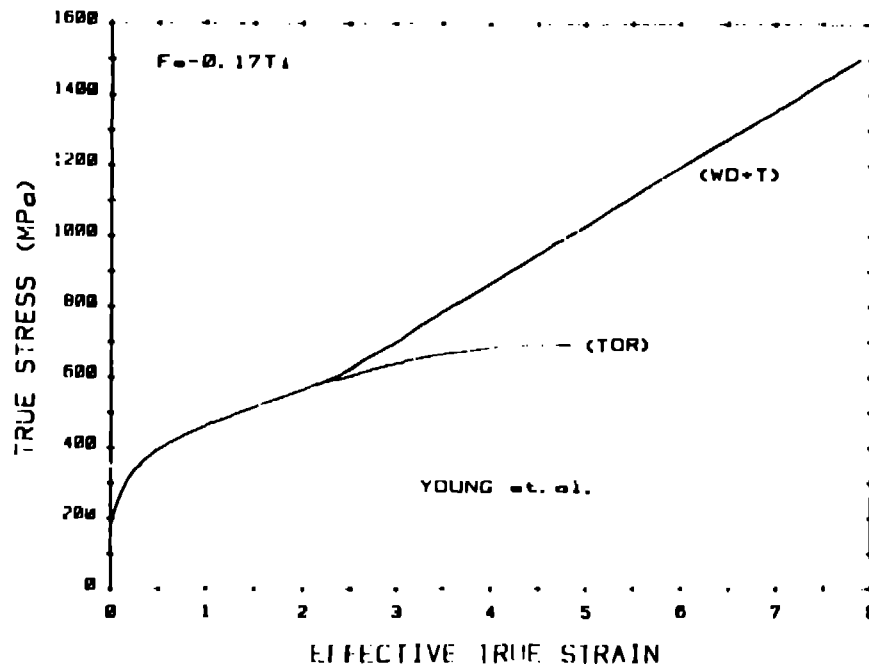


Fig. 13. Comparison of stress-strain curves for Fe-0.17% Ti deformed by torsion and wiredrawing + tension. (Reference 33.)

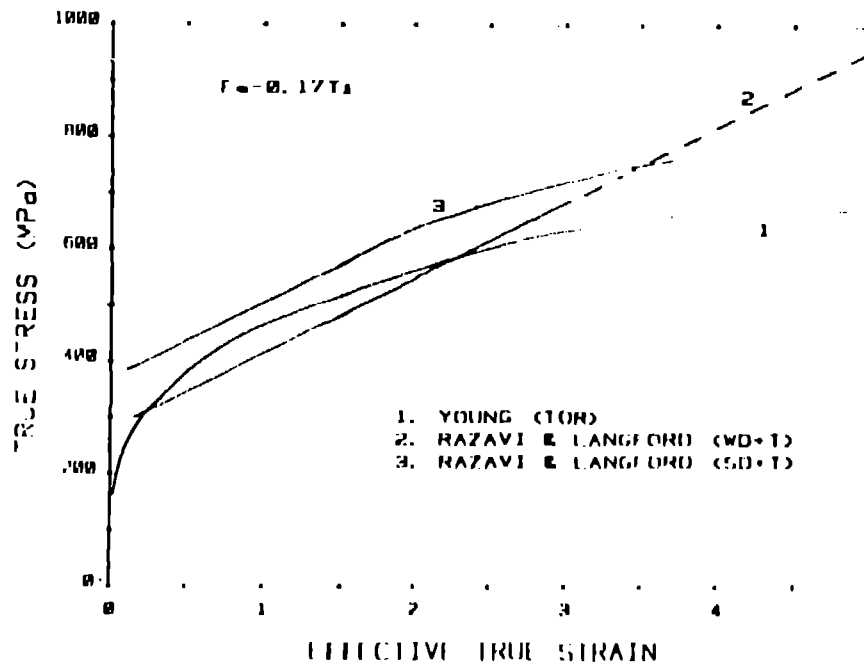


Fig. 14. Comparison of stress-strain curves for Fe-0.17% Ti deformed by torsion, wiredrawing, and strip drawing. The dashed line is a linear extrapolation of Razavi and Langford's data based on other literature values. (References 33, 34.)



direction and, hence, the probability of annihilation of dislocations of opposite sign in cell or subgrain boundaries is large. This results in a low flow stress and the tendency for saturation. In axisymmetric deformation the number of different slip systems is always at least four and, hence, the probability of annihilation less.

The response of multiphase materials to large deformation was also reviewed by GVA.<sup>1</sup> Here we only want to add the recent results of Aghan and Nutting<sup>38,39</sup> on high-sulfur and lead-bearing steels rolled at room temperature. The flow curves shown in Fig. 15 show a dramatic increase at very large strains. In the case of the high-sulfur steel the MnS inclusions are more plastic than the matrix and, at large strains, a fiber reinforcing effect increases the flow stress above that of plain carbon steel. In the lead-bearing steel, lead causes the MnS particles to fragment and less reinforcing effect is realized. We use these examples to demonstrate the important role that second-phase particles can have on the flow stress at large strains without having much influence at small strain.

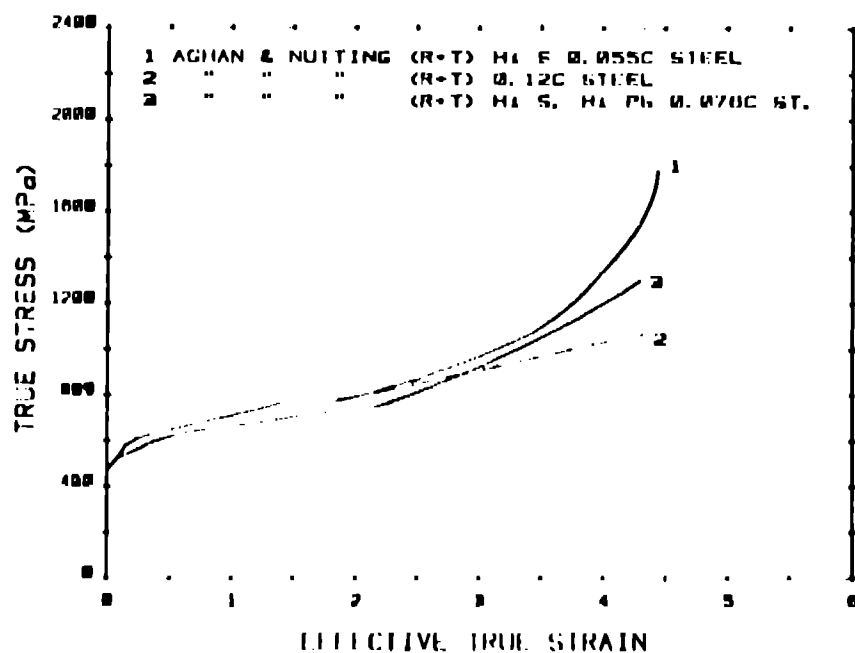


Fig. 15. Stress-strain curves for low-carbon steel (#2), high-sulfur steel (#1), and high-sulfur, leaded steel (#3). (References 38, 39.)

## DISCUSSION

The results presented here and those reviewed by GVA<sup>1</sup> and Hecker, Stout, and Eash<sup>2</sup> indicate that saturation (steady state behavior) of the flow stress in fcc materials is not universal. Steady state behavior should be expected if the evolution of substructure is controlled only by undisturbed dislocation interaction. However, as pointed out by Mecking and Grinberg,<sup>41</sup> many potential disturbing influences may appear at large strains. These include i) grain size effects, ii) deformation bands, iii) surface effects, iv) strain-induced transformations (twinning or martensite) v) changing deformation mode, vi) deformational instabilities such as shear bands, vii) texture development, and viii) second-phase particles. As a result of these disturbing influences we find that continued hardening is generally observed. High purity and torsional deformation modes favor steady state and saturation.

The effects of material purity is demonstrated convincingly above. As explained, solute atoms retard the recovery process, shifting the balance between dislocation generation and annihilation to larger strains. Alloying can have similar effects or introduce much greater complexities by the interaction of dislocations with complex microstructures such as those demonstrated for Al-4% Cu alloys (Fig. 4). The influence of grain size remains much stronger at large strains than expected (Fig. 5). Also, as indicated in Fig. 9 grain boundaries may again become important structural elements at very large strains and, perhaps, explain the peculiar hardening behavior of nickel (Fig. 8).

The evolution of texture most likely plays a significant role in controlling the flow behavior. Our experiments on brass indicate that the difference between axisymmetric and torsional deformation at  $\epsilon_{eff} = 0.4$  can be explained qualitatively on the basis of texture development. A quantitative comparison awaits the type of rigorous analysis of texture prediction being conducted by Jonas et al.<sup>42</sup> Results for bcc materials also indicate potential textural effects. If texture plays a major role in hardening, then the likelihood of finding a single, intrinsic hardening curve for polycrystalline materials is small because deformation geometry will influence the results.

Twinning, deformation bands, and shear bands all have been studied microscopically. The role that these mechanisms play in

hardening has not been established quantitatively. Second phase particles can play an important role in hardening. In Al-Fe or Al-Ni alloys they stabilize the size of the substructure. In steels containing high sulfur or lead additions they can produce a fiber reinforcing effect at very large deformations.

#### SUMMARY

Strain hardening at large plastic strains cannot be inferred from small-strain tensile tests. Most metals and alloys at room temperature do not reach steady state saturation at strain levels of 3 to 5. Typically, some disturbing influence offsets the balance between dislocation generation and annihilation. The most prominent of these appears to be texture formation. However, grain size, second-phase particles, and deformation on shear bands are also important. The effect on hardening of most of these features depends on geometry (or deformation mode) and, hence, no single intrinsic hardening curve can be expected at large strains. It should be noted that high material purity and a torsional deformation mode favor saturation.

#### ACKNOWLEDGMENTS

This work was sponsored by the Division of Materials Sciences, Office of Basic Energy Sciences, U. S. Department of Energy.

#### REFERENCES

1. J. Gil Sevillano, P. van Houtte, and E. Aernoudt, Large Strain Work Hardening and Textures, *Prog. Mater. Sci.*, 25, pp. 69-412 (1980).
2. S. S. Hecker, M. G. Stout, and D. T. Eash, Experiments in Plastic Deformation at Finite Strains, *Proc. of Workshop on "Plasticity of Metals at Finite Strains: Theory, Experiment and Computation,"* held at Stanford University, CA, June 29, 30 and July 1, 1981.
3. C. S. Hartley, and D. A. Jenkins, Tensile Testing at Constant True Strain Rates, in: "Proceedings of 6th International Conference on Experimental Stress Analysis", Munich, W. Germany, pp. 379-383 Sept. 18-22 (1978).

4. C. S. Hartley, D. A. Jenkins, and J-J. Lee, Strain Dependence of Strain-Rate Sensitivity in: "Proceedings of 5th International Conference on Strength of Metals and Alloys", P. Haasen, V. Gerold, and G. Kostorz, eds. Pergamon Press, pp. 523-528 (1980).
5. Z. Marciniak, and K. Kuczynski, Limit Strains in the Processes of Stretch-Forming Sheet Metal, Int. J. Mech. Sci., 9, pp. 609-620 (1967).
6. S. P. Keeler, and W. A. Backofen, Plastic Instability and Fracture in Sheets Stretched Over Rigid Punches, Trans. ASM, 56, pp. 25-48 (1963).
7. M. Azrin, and W. A. Backofen, The Deformation and Failure of Biaxially Stretched Sheet, Met. Trans., 1, pp. 2857-2856 (1970).
8. A. K. Ghosh, and W. A. Backofen, Strain Hardening and Instability in Biaxially Stretched Sheets, Met. Trans., 4, pp. 1113-1123 (1973).
9. A. J. Ranta-Eskola, Use of the Hydraulic Bulge Test in Biaxial Tensile Testing, Mech. Sci., 1, pp. 457-465 (1979).
10. R. Bell, J. L. Duncan, and I. H. Wilson, A Sheet-Bulging Machine with Closed Loop Control, J. Strain Anal., 2, pp. 246-253 (1967).
11. M. G. Stout, and S. S. Hecker, Comparison of Plastic Instability in Sheet and Tubular Specimens of 70-30 Brass, presented at Fall TMS/AIME Meeting, Louisville, Ky Oct. 13, 1981. Abstract in J. Metals, 33, p. 21 (1981).
12. A. Nadai in: "Theory of Flow and Fracture", 2nd ed., McGraw Hill Book Company Inc., 1, p. 349 (1950).
13. D. S. Fields, Jr., and W. A. Backofen, Determination of Strain Hardening Characteristics by Torusion Testing, Proceedings ASTM, 57, pp. 1259-1272 (1957).

14. G. R. Canova, S. Shrivastava, J. J. Jonas, and C. G'Sell, The Use of Torsion Testing to Assess Material Formability, Prepared for presentation at the ASTM Symposium "Formability-2000," Chicago, Ill. (1980).
15. F. A. Hodierne, A Torsion Test for Use in Metalworking Studies, J. Inst. Metals, 91, pp. 267-273, 1963.
16. S. S. Hecker, D. L. Rohr, and R. M. Aikin, Unpublished work Los Alamos National Laboratory (1978).
17. P. E. Armstrong, J. E. Hockett, and O. D. Sherby, Large Strain Multidirectional Deformation of 1100 Aluminum at 300 K, J. Mech. Phys. Sol., 30, pp. 37-58 (1982).
18. S. K. Varma, and B. G. LeFevre, Large Wire Drawing Plastic Deformation in Aluminum and Its Dilute Alloys, Met. Trans. A, 11A, pp. 935-942 (1980).
19. D. Kalish and B. G. LeFevre, Subgrain Strengthening of Aluminum Conductor Wires, Met. Trans. A, 6A, pp. 1319-1324 (1975).
20. H. Luthy, A. K. Miller, and O. D. Sherby, The Stress and Temperature Dependence of Steady-State Flow at Intermediate Temperatures for Pure Polycrystalline Aluminum, Acta Met., 28, pp. 169-177 (1980).
21. J. Nuttall, and J. Nutting, Structure and Properties of Heavily Cold-Worked fcc Metals and Alloys, Metal Sci., 12, pp. 430-437, 1978.
22. B. Nourbakhsh and J. Nutting, The High Strain Deformation of an Aluminum -4% Copper Alloy in the Supersaturated and Aged Conditions, Acta Met., 28, pp. 357-365, 1980.
23. D. J. Lloyd, and D. Kenny, The Structure and Properties of Heavily Cold Worked Aluminum Alloys, Prepublication paper from Aluminum Company of Canada, Ltd. Research Center, Kingston, Ontario, Canada.
24. D. J. Lloyd, Deformation of Fine-Grained Aluminum Alloys, Metal Sci., 14, pp. 193-198 (1980).

25. G. I. Taylor, and H. Quinney, Proceedings of the Royal Society of London, 143, p. 307 (1934).
26. O. D. Sherby, and C. M. Young, Some Factors Influencing the Strain Rate-Temperature Dependence of the Flow Stress in Polycrystalline Solids, in: "Rate Processes in Plastic Deformation of Materials", J. C. M. Li, and A. K. Mukherjee eds., ASM, pp. 497-541 (1975).
27. J. H. Cairns, J. Clough, M. A. P. Dewey, and J. Nutting, The Structure and Mechanical Properties of Heavily Deformed Copper, J. Metals, 99, pp. 93-97 (1971).
28. W. G. Truckner, and D. Lakkola, Strengthening of Copper by Dislocation Substructures, Met. Trans. A, 8A, pp. 45-49, (1977).
29. P. E. Armstrong, Los Alamos National Laboratory, (1979), unpublished work.
30. W. H. Zimmer, S. S. Hecker, L. E. Murr, and D. L. Rohr, Large-Strain Plastic Deformation of Commercially-pure Nickel, accepted for publication in Metal Sci. (1980).
31. A. K. Ghosh, Plastic Flow Properties in Relation to Localized Necking in Sheets, in: "Mechanics of Sheet Metal Forming-Material Behavior and Deformation Analysis", D. P. Koistinen, and N-M. Wang, eds., pp. 287-312, Plenum Press (1978).
32. R. H. Wagoner, Plastic Behavior of 70-30 Brass Sheet, Met. Trans. A, 13A, pp. 1491-1500 (1982).
33. C. M. Young, L. J. Anderson, and O. D. Sherby, On the Steady State Flow Stress of Iron at Low Temperatures and Large Strains, Met. Trans., 5, pp. 519-520 (1974).
34. A. Razavi, and G. Langford, Strain Hardening of Iron: Axisymmetric vs. Plane Strain Elongation, in: "Proceedings of 5th International Conference on Strength of Metals and Alloys", P. Haasen, V. Gerold, and G. Kostorz, eds., pp. 831-836, Pergamon Press (1980).

35. E. Aernoudt, and J. Gil Sevillano, Influence of the Mode of Deformation on the Hardening of Ferritic and Pearlitic Carbon Steels at Large Strains, J. Iron and Steel Inst., 211, pp. 718-725 (1973).
36. J. Gil Sevillano, and E. Aernoudt, On the Influence of the Mode of Deformation on the Hardening of Iron at Low Temperature and Large Strains, Met. Trans. A, 6A, pp. 2163-2164 (1975).
37. C. M. Young, L. J. Anderson, O. D. Sherby, reply to "On the Influence of the Mode of Deformation on the Hardening of Iron at Low Temperature and Large Strain," Met. Trans. A, 6A, pp. 2164-2165 (1975).
38. R. L. Aghan, and J. Nutting, Structure and Properties of Free-Cutting Steels After Deformation to High Strains, Metals Tech., 8, pp. 41-45 (1981).
39. R. L. Aghan, and J. Nutting, Structure and Properties of Low-Carbon Steel After Deformation to High Strains, Metal Sci., 14, pp. 233-237 (1980).
40. J. Weertman and S. S. Hecker, Theory for Saturation Stress Difference in Torsion versus Other Types of Deformation at Low Temperatures, submitted to J. Mech. Mater. (1982).
41. H. Mecking and A. Grinberg, Discussion on the Development of a Stage of Steady-State Flow at Large Strains, in: "Proceedings of 5th International Conference on Strength of Metals and Alloys", P. Haasen, V. Gerold, and G. Kostorz, eds., pp. 289-294, Pergamon Press, (1980).
42. J. J. Jonas, G. R. Canova, S. C. Shrivastava and N. Christodoulou, Sources of the Discrepancy Between the Flow Curves Determined in Torsion and in Axisymmetric Tension and Compression Testing, Proc. of Workshop on "Plasticity of Metals at Finite Strains: Theory, Experiment and Computation," held at Stanford University, CA, June 29, 30 and July 1, 1981.